LANGMUIR

pubs.acs.org/Langmuir Article

The Interaction and Lift-Off Forces of an Atomic Force Microscope Tip from Single Fibers Extracted from Protective Clothing Fabric

Ronald G. Reifenberger and Candace Su-Jung Tsai*

Cite This: *Langmuir* 2024, 40, 14788−14797 Read Online

ABSTRACT: The widespread use of engineered nanoparticles (ENPs) poses a potential health hazard to humans, especially to those involved in either nanoparticle manufacturing or the usage and assembly of a final product. In this study, we performed systematic force vs distance experiments ($F(z)$) using an atomic force microscope (AFM) on fibers commonly used in street clothing and protective laboratory clothing to better characterize the relevant interaction forces between engineered nanoparticles (ENPs) and the contacted fabric fibers. The intent of this study is to identify those factors that influence the interaction of ENPs with fabrics with an aim to improve the efficacy of protective clothing against ENP exposure and mitigate potential health risks. A ∼14 nm diameter AFM SiO_x tip (with nanoscale radius of curvature) is considered as an effective oxide ENP. Features present (or absent) in a well-executed $F(z)$ AFM experiment provide a fingerprint that distinguishes the relevant forces and interaction mechanisms in play. Measurements of $F(z)$ as a function of relative humidity were also performed to assess the importance of thin surface water layers in binding nanometer-size oxide ENPs to a fabric fiber. The $F(z)$ data indicate the dominant mechanism for adhesion of the oxide tip to the various fabric fibers (cotton, Tyvek (HD polyethylene), polypropylene, and polyester) can be attributed to a van der Waals interaction. The analysis provides no evidence for long-range electrostatic forces or capillary-induced adhesion of the AFM tip to the fibers studied.

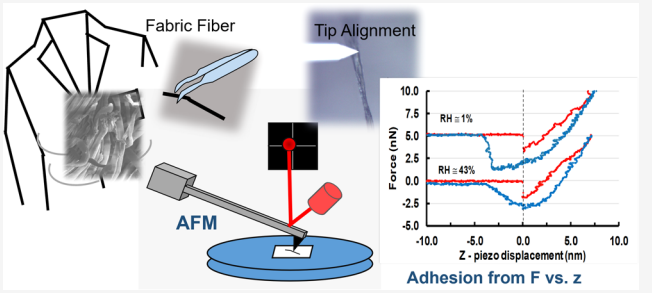

INTRODUCTION

Since the mid-1990s, the use of Engineered Nanoparticles (ENPs) has grown steadily. Countless studies have repeatedly shown that ENPs improve performance in products spanning a wide variety of different business sectors. As a result, ENPs have found extensive use in additives, coatings, specialized industrial components, pharmaceuticals, and structural materials. The widespread availability of ENPs poses a potential health hazard to humans, especially to those involved either in their manufacture or the use and assembly of a final product. There is a general awareness that fine particles designated as $PM_{2.5}$ are widely dispersed in the environment.[1] These fine particles with a diameter of 2.5 μm or less come from a wide variety of sources such as ENPs from production and usage, nanoplastics produced by the fragmentation of plastic debris, particulates in auto exhausts, and smoke produced by wildfires. This nanoscale waste continues to cause concern[2] as evidenced by the steady increase in burdensome regulatory laws designed to curtail their use.

One way to ease public apprehension regarding potential ENP risks might be to better optimize the overall efficacy of clothing that protects against ENP exposure by making a rational choice of fabrics that more efficiently repel ENPs or attract and trap them. This idea reinforces the growing sentiment that fabric for clothing in and of itself constitutes a complex material system. As such, the challenge in the fabric industry to develop more effective protection against ENPs tends to be multidisciplinary, requiring a truly interdisciplinary approach to achieve meaningful progress.[3]

A question that begs to be answered is how to select a particular fabric to help mitigate risk for a specific genre of ENPs. Can an optimal fabric be identified that will maximize protection against exposure to different types of ENPs? Definitive answers to this question might well become an innovative driver in future clothing design. Recent work that takes a first step in quantifying exposure of different fabrics to controlled contamination by aluminum oxide ENPs, carbon ENPs and carbon nanotubes has recently been reported.[4,5] In this work, the retention of these different ENPs to both as-received and surface treated fabrics were quantified.

The study reported below is intended to extend the previous work by probing the nature and strength of the physical interaction between an AFM tip (with nanoscale radius of curvature), considered as an effective oxide ENP, with different

Received: December 19, 2023
Revised: June 28, 2024
Accepted: July 3, 2024
Published: July 10, 2024

fabrics commonly used to make street and protective clothing. Although the AFM tip cannot accurately capture the surface activity, mobility, or clustering of nanoparticles, the nanoscale curvature of the AFM tip is thought to approximate the essential aspects of the ENP-substrate interaction that one might expect for an isolated ENP on a particular substrate of interest.[6−9] The motivation behind this investigation is a first step in providing information for a rational selection of a fabric fiber type for a specific application.

The aim of this work is not to perform AFM indentation studies on polymeric fabric fibers and extract information about the elastic properties of the fiber materials. Rather we try to provide some much-needed information about relative tip lift-off forces from different fabric fibers. We also establish the nature of the AFM tip-fiber interactions. Any such information might provide a more basic and fundamental understanding of how oxide ENPs adhere to different fabrics, thereby laying the groundwork for further studies as well as the continued optimization of smart textiles in the future.

The primary tool employed in this study is the Atomic Force Microscope (AFM). The AFM measures the interaction of a sharp tip integrally attached to a flexible microcantilever as the tip is made to approach, contact, indent and then withdraw from the surface of a fabric of interest. The underlying premise behind our work is that an oxidized SiO_x AFM tip of ∼14 nm diameter serves as an effective oxide ENP (silica). For ENPs with diameters in this size range, simple considerations suggest that the relevant forces acting on an ENP near a fabric surface will be on the order of 10^{-9} Newtons, well within the range of accurate measurement by an AFM. By quantifying the forces acting on an AFM tip, we intend to provide a window to view relevant forces acting on an ENP in the same nanometer size range. With this context in mind, it seems natural to broadly discuss what AFM experiments can reveal about ENP/fabric interactions.

Since the AFM was first introduced in 1986,[10] this scanning probe technique has enjoyed widespread use in every branch of science and engineering. The characterization of polymer surfaces with an AFM has been reported over 25 years ago.[11] More recent work with an extensive list of literature citations has summarized the use of an AFM to probe polymer structure and properties.[12] Only a few reports have appeared where an AFM has been used to study textiles.[13−22] Topics that have been reported are extensive and diverse, and include studies of the microstructure of woven fabrics, a characterization of hydrophobic/hydrophilic coatings applied to textiles, maps of the variations in the surface charge on wool, and the use of nanocomposite coatings designed to produce antibacterial fabrics.

A well-established facet of many AFM experiments is to acquire $F(z)$ data in which the force F acting on an AFM tip is measured as the separation distance z between the tip and substrate is systematically and controllably reduced. The ability to perform this measurement with nanoscale spatial resolution makes $F(z)$ data an invaluable probe of the mechanical properties of materials. Although characterizing the properties of the base material comprising each of the fabric fibers is not the main interest in this study, features present (or absent) in a well-executed $F(z)$ experiment provide a sample-dependent fingerprint that characterizes the relevant forces and interaction mechanisms in play.

Our main goal is to study the tip−substrate forces as a SiO_x AFM tip approaches and makes contact to a fabric surface. Considerable insight can be gained about (i) the strength of the tip-fabric interaction, (ii) the fundamental origin of the interaction, (iii) the influence of an uncontrolled surface layer, including a layer of protruding microfibers, that might coat the fabric surface, (iv) time-dependent viscoelastic effects that develop after the tip contacts a fabric fiber, and (v) estimates of the force required to remove the oxide AFM tip from a particular fabric.

The AFM work described in what follows quantitatively probes the basic nature and strength of interaction of nanometer-size oxide ENPs with a variety of different fabrics commonly used to make protective clothing. Of particular interest is to identify those fabrics that most strongly trap ENPs to minimize ENP spread and ENP resuspension.

METHODS

To assess the adhesion of oxide ENPs to different fabrics, an AFM study was performed on single fibers obtained from two woven and two nonwoven fabrics used for lab coats, all purchased through Global Industrial: 100% cotton (Fashion Seal men's lab coat), polyester/cotton blend (80% polyester 20% cotton, Red Kap women's button closure lab coat), Tyvek (HD polyethylene, Dupont), and 100% polypropylene (Keystone HD polypropylene lab coat).

As detailed elsewhere, X-ray photoelectron spectroscopy (XPS) and water contact angle goniometry have been performed on identical as-received fabrics to characterize relevant surface chemistry and wettability linking hydrophobicity level.[5] Briefly, as expected, the chemical compositions inferred from the XPS data indicate that polypropylene and Tyvek fabric were primarily carbon, while the 100% cotton and the cotton/polyester blend fabrics had increased O % with evidence for additional binding environments related to oxygen.

The cotton/polyester fabric showed a 4.8% Si content, suggesting that this material had been treated with a silicon-based softener commonly used during the production of garments made from rougher materials (e.g., polyester). High-resolution C 1s XPS spectra for all the as-received fabrics are consistent with carbon in environments corresponding to C−C/C−H, C−O, and C═O bonding. As expected for the polypropylene and Tyvek fabrics, no C═O functionality was measured, and these samples contained the smallest amount of C−O functionality. Cotton-containing fabrics showed elevated amounts of oxygen bound to carbon, consistent with the chemical structure of cotton.

The fabrics used to make these lab coats meet different needs. For example, cotton fabric tends to be comfortable, lightweight, and long-lasting. They are the preferred material for most street clothing and lab coats by most scientists. Although not as soft and breathable as 100% cotton, polyester-cotton blends often find use in common clothing and in a setting without open flames. For an extremely durable, rip and tear-resistant lab coat, Tyvek is often the fabric of choice. Coats made from Tyvek typically find use for protection against airborne biological and radioactive materials. Polypropylene garments find widespread use for disposable clothing, in biomedical laboratories where pathogen protection and cross-contamination are a concern. Because of the relatively low melting temperature of polypropylene (160 °C), the fabric is generally not suitable in settings where high temperatures are routinely encountered. Coats made from this synthetic fiber are relatively inexpensive and often considered a disposable item.

A table listing a few properties of the base polymers used to manufacture each fabric fiber is given in Table 1. Other fabric material properties, including scanning electron microscopy (SEM) images included in Supporting Information (SI) Figure S1, are given in our previously published results.[4,5] Figure S2 shows the fabric fiber under high magnification. The density listed is the bulk density of the base material and is given here as a rough guide to the relative packing density of the molecular chains in each fabric fiber. The resulting areal density of the fabric itself is related to the material bulk density but is

https://doi.org/10.1021/acs.langmuir.3c03939
Langmuir 2024, 40, 14788−14797

Table 1. A Selected List of the Base Polymer Properties for the Fabrics Studied

fabric	chemical formula	density (g/cm^3)	melting temp.	bulk Young's modulus (GPa)
cotton[a]	$[-C_6H_{10}O_5-]_n$	1.35	N/A	5.5−12.6
polyester (PET)	$[-C_{10}H_8O_4-]_n$	1.38	220 °C	3.8
Tyvek[b]	$[-C_2H_4-]_n$	0.93−0.97	130 °C	1.0
polypropylene	$[-C_3H_6-]_n$	0.90	160 °C	0.8

[a]Cotton is primarily cellulose; [b]Tyvek is HD polyethylene.

ultimately determined by the fabrics' porosity which depends on the weave. Typical values of Young's modulus of the bulk material are also listed to provide a convenient scale when judging the relative mechanical strength of each fiber.

From the start, we did not harbor the illusion that an individual fiber would provide an ideal sample comprised solely of the base polymer having a uniform and chemically homogeneous surface. We anticipated that uncontrolled variability would characterize the data acquired from a randomly selected nanoscale region of an individual fiber. Thus, our AFM study described below will focus on trends related to attractive forces, adhesive forces, and the nature of the tip/fabric fiber interaction rather than on obtaining precise and statistically significant values for any particular quantity of interest.

Facilities and Equipment. Throughout the course of this study, an Asylum Research AFM Cypher Model S was used. After inserting a fiber sample and cantilever into the Cypher AFM, the front door of a metallic enclosure surrounding the AFM was closed to ensure a stable thermal equilibrium. The temperature inside the electrically shielded thermal enclosure box was unregulated and was typically measured to be 26 ± 1 °C.

The relative humidity (RH) (25−30%) and temperature in the lab room itself were determined by standard HVAC building controls. The metal enclosure box surrounding the AFM could be purged using high purity dry N_2 gas to allow data acquisition at a reduced humidity level. The RH was measured to an accuracy of ∼1% with a Pyle hand-held PTHM20 m that could be placed directly inside the enclosure box. Once a N_2 purge was initiated, it required about 30 min for the humidity inside the AFM enclosure box to reach a value less than 2%.

Experimental Procedures. *AFM Considerations.* AFM micro-cantilevers, Model AC240TS-R3 (available from Asylum Research), were used throughout. These AFM levers (nominal dimensions of 240 μm × 40 μm × 2.3 μm) typically have a resonant frequency near 70 kHz and a spring constant between 2 and 3 nN/nm. The tip length is ∼14 μm long, ending in a SiO_x tip with a nominal diameter specified by the manufacturer to be 14 nm. The manufacturer of these AFM cantilevers does not provide an estimate for the uncertainty in the tip radius, but a few careful studies have been carried out that provide useful estimates. Although the identity of the AFM probes that were characterized is not revealed, Maragliano et al. find that an AFM probe with a nominal radius of 8 nm has an uncertainty of ±3 nm.[23] Thus, it might be expected that the cantilevers used in our study (ACS240TS-R3) would have a similar uncertainty.

Before use, each cantilever was exposed to ∼10 min of ultraviolet (UV) radiation produced by an "AFM Probe Tip Cleaner" (SPI Supplies) to reduce any possible hydrocarbon contamination. After this treatment, the UV lamp produced a noticeable odor of ozone. The individual spring constant k for each cantilever was calibrated using the well-established thermal method that measures the k_BT room temperature thermal vibration spectrum of the cantilever.[24] Relying on the fluctuation dissipation theorem and combining with Sader's hydrodynamic damping method,[25] a reliable value for k as well as the inverse optical lever sensitivity (invOLS) for each cantilever was obtained. Once the spring constant is known, the cantilever deflection q (what the AFM measures) can be converted to an applied force using eq 1.

$$F_{cant} = kq \quad (1)$$

Sample Preparation. Preliminary AFM imaging experiments on the as-received fabric materials proved very unreliable due to randomly protruding fibers that ensnared and often snapped off the AFM cantilevers. We therefore decided to study individual fibers that were carefully extracted from the fabric of each lab coat. The exception was the Tyvek lab coat fabric, which is made by compressing randomly placed, high density polyethylene fibers to make a nonwoven, flexible, and tough fabric material. Therefore, the Tyvek fabric surface itself was studied with no attempt to isolate, extract and mount an individual high-density polyethylene fiber.

In preparation for the AFM studies, an individual fiber around 5 to 10 mm in length was carefully extracted from each fabric using tweezers under an optical microscope. An individual fiber typically had a diameter between 10 and 25 μm, making the fiber diameter about 700−1400 times greater than the diameter of the AFM tip. The synthetic fibers (polyester and polypropylene) appeared to have a uniform cross-sectional diameter when viewed under a compound optical microscope (adjustable magnification between 7.5× to 30×). These fibers were visibly kinked due to their prior inclusion into the woven fabric material. The natural cotton fibers, when viewed under the optical microscope, had both a kinked and twisted appearance which gave a clear visual impression of a nonuniform cross-sectional area.

After extracting a single fiber from each fabric, the fabric fiber was placed on a clean, thin steel mounting disc having a diameter of ∼15 mm. Except for Tyvek, all the fibers had a permanent "corkscrew" shape because they were extracted from individual threads that had been twisted and woven to make a fabric. Each end of the fiber was firmly held to the supporting steel disc by a tiny drop of glue. The corkscrew shape caused the fiber to periodically touch the mounting disk about once every millimeter between the two glue drops, providing additional support for the fiber along its length. Rough estimates of the suspended fiber deflection caused by applying a point load of 5 nN to the middle of a 1 mm section of the supported fiber gave a calculated fiber displacement of ∼1 nm. To minimize this deflection, data were taken by positioning the cantilever over the fiber close to a glue drop which provided a rigid support point.

Each disc was given a unique sample label to allow ready identification at a later date. Once prepared, the mounted samples were stored in labeled boxes which were kept inside a covered desiccator that was backfilled with dry N_2 gas for the duration of the entire study. No attempt was made to further clean the mounted fabric fiber.

Tip-fiber Alignment. The steel support disc with mounted fiber was magnetically clamped when inserted into the AFM. This magnetic clamping allowed the disc to be laterally translated in steps of a few micrometers (using a stick/slip inertial translation mechanism) until the individual fiber could be approximately positioned beneath the AFM cantilever. This initial rough alignment was facilitated using the Cypher's view module which includes a Pixelink camera with an Olympus LUCPlanFL objective having a magnification of 20×. After this rough alignment was initially made, the AFM system was allowed to thermally stabilize for ∼1/2 h before taking data.

F(z) Considerations. After reaching thermal equilibrium, a more precise alignment of the tip over the fiber was performed as shown in Figure 1. A discussion of the constraints of the AFM tip alignment above the apex of the fiber can be found in the SI Tip Alignment Issues Section (see Figure S3). Following this final alignment, a sequence of $F(z)$ measurements was executed under ambient conditions.

A typical $F(z)$ measurement relies on a calibrated Z-piezoelectric translator to move the fabric fiber toward the tip at a user defined approach speed which, in this study, was typically set to a value between 25 and 50 nm/s. During an $F(z)$ experiment, the Z-displacement of the fiber with respect to the tip is digitized, along with the cantilever's deflection $q(Z)$, at a user determined rate which, in this study, was typically set to 2 kHz. The AFM electronics accurately

https://doi.org/10.1021/acs.langmuir.3c03939
Langmuir 2024, 40, 14788−14797

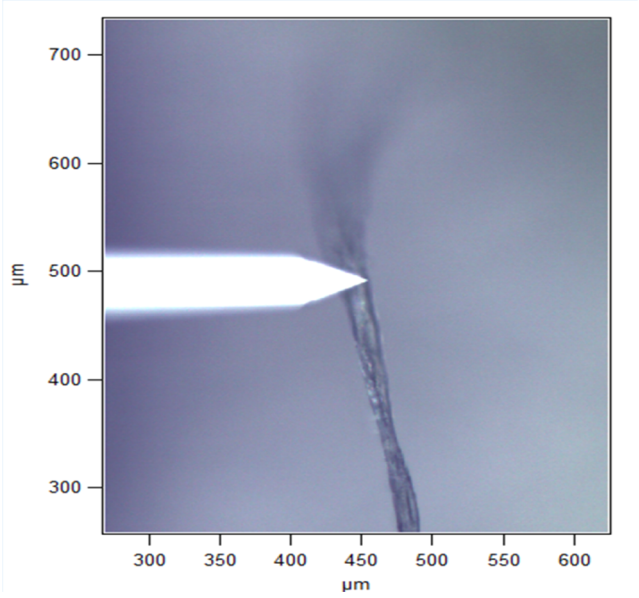

Figure 1. A photo of the top side of an AFM AC240TS-R3 microcantilever positioned above a cotton fiber. The AFM tip is located on the bottom side of the cantilever and is not visible in this view. Due to the limited depth of field of the optical microscope, the downward slant of the twisted cotton fiber makes it appear out of focus on the section of the fiber located above the cantilever.

measured the cantilever deflection using a laser beam bounce technique to infer the force F on the tip using eq 1.

When the tip is not in contact with the fiber and when no long-range forces are present, the tip-fiber separation distance d is accurately tracked (to within a constant unknown offset) by the piezo displacement Z. Once the tip jumps into contact with the fiber surface, the tip-fiber separation becomes a small value (a_o) determined by the relevant atomic spacing for the tip-fiber system. Thus, $d = a_o$ for the remainder of the experiment. After contact is established, the Z-piezo continues to move until the cantilever passes through its original undeflected position ($q = 0$), implying that the force applied by the cantilever also returns to 0. While this zero-force condition generally holds true for hard substrates, for softer materials it becomes questionable. Because the undeflected cantilever condition is easy to determine, in what follows, we will use it to define the point where $d = 0$.

After contact, as the Z-piezo continues to move, the measured cantilever deflection now becomes a combination of cantilever bending and indentation. After $F(Z)$ data has been acquired, it is relatively easy to remove the cantilever bending from the data,[26] resulting in $F(d)$ data which measures the fiber deformation as a function of cantilever force. After contact, once the conversion from Z to d is made, the resulting $F(d)$ will show the force required to achieve a given deformation δ.

In what follows, forces plotted as positive are considered repulsive, while forces plotted as negative are considered attractive. Typically, between 10,000 to 30,000 data points were digitized for each $F(z)$ measurement, depending on how far the tip was initially positioned above the fiber. After the experimental study of a particular fiber was completed, the conversion from Z to d, (and δ) was performed, and the relevant data subset was selected for further analysis.

Every fiber was studied at least twice to ensure reproducibility of results. Reproducibility issues are discussed further in the SI Reproducibility of $F(z)$ data section, Table S1 and Figure S4. For each fiber, $F(z)$ data were systematically acquired for specified set point forces of 2, 5, and 10 nN. These low set point forces were intentionally chosen because our interest is primarily to study how ENPs interact with a fiber surface. Presumably, an adsorbed ENP does not indent the surface on which it rests, so high set-point forces are not of interest. In addition, other factors that influenced the decision to use low loading forces included the desire (i) to minimize plastic deformations that might be caused by larger indentations and (ii) to reduce the chances of tip damage and wear. Thus, the experiments are specifically designed to characterize the interaction of an ENP with the surface of a fiber with a minimum indentation, thereby providing some information about how an ENP interacts and binds to fibers in fabric.

The tip-fiber interaction can be influenced by residual surfactants, stabilizers, solvents, spinning agents, or plasticizers that unevenly coat individual fibers in the fabric. Our goal is to study the fibers as received, since this is how the fabrics are deployed for use. From prior studies, we anticipated that the small AFM set-point forces used in our work might produce a depth-dependent elastic modulus, an effect that is sometimes referred to as a skin effect.[27] As the indentation increases, an elastic modulus more characteristic of the base material value is expected. For these reasons, we do not anticipate our measured mechanical properties (e.g., Young's modulus) will necessarily match those values commonly cited in the literature for the base polymer materials (see Table 1).

Data Analysis. During the course of this study, a total of about 750 $F(z)$ data sets were acquired under ambient conditions and in a dry N_2 environment (RH < 2%). The substrates were individual fibers extracted from the fabrics composed of 100% cotton, polypropylene, 80:20% polyester/cotton (polycotton), and the surface of Tyvek. The interpretation of $F(d)$ data obtained using an AFM is well established and can be found elsewhere.[26,28−30] By comparing the shape of selected regions of the $F(d)$ data, inferences about the relative stiffness (hard or soft), relative adhesion (low or high), and relative deformation (elastic or plastic) of a set of fabric fibers can be made.

RESULTS AND DISCUSSION

Representative $F(d)$ Data for all Fibers. Figure 2 shows representative $F(d)$ data taken under ambient conditions for all fibers plotted on one graph. The data plotted were carefully selected following the criteria laid out in the SI. The results were obtained under ambient condition using different AC240TS-R3 AFM cantilevers. The set-point force (the maximum applied force) for each curve is small and nominally the same, i.e., 5 nN. Note that all the $F(d)$ data acquired during this study are plotted using the same color convention: a red curve represents data as the tip approaches or indents the fabric fiber while the retract data are plotted as blue.

All the data in Figure 2 show a few common characteristics that deserve comment. Starting with the approach (red) data near $d \cong -20$ nm, the tip is far from the fiber, and there is no force acting on the tip as represented by the appearance of a flat, red horizontal line. Under these conditions, there is no cantilever bending and $d = Z$. Note that if a significant long-range force (e.g., from electrostatics) were present, the approach curve would have a noticeable upward or downward slope depending on whether the electrostatic force was repulsive or attractive.

When the fiber approaches within ∼5 nm of the tip ($d = -5$ nm), the tip begins to feel an attractive force and abruptly jumps into contact with the fiber. This occurs when the gradient of the interaction force between tip and fiber overcomes the restoring force offered by the bent AFM cantilever. In Figure 2, this is observed as a discontinuous jump downward (a negative force implies an adhesive attractive force). To a first approximation, the size of this jump indicates the strength of interaction between the tip and substrate and is related to the relevant Hamaker constant that characterizes the surface interaction. This jump to contact feature was barely discernible for the Tyvek fabric, indicating a relatively weak

https://doi.org/10.1021/acs.langmuir.3c03939
Langmuir 2024, 40, 14788−14797

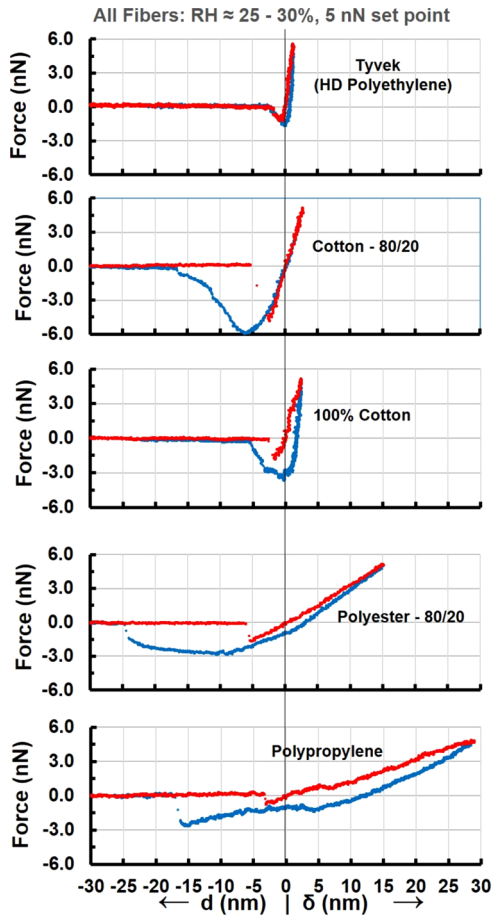

Figure 2. A collection of $F(d,\delta)$ data for all fibers studied under ambient conditions (RH between ~25 to ~30%). All data have a nominal 5 nN set-point force (maximum applied force) using an AFM cantilever with a SiO_x tip having a nominal diameter of 14 nm and a nominal spring constant $k \sim 2$ N/m. Red represents the tip approaching the fiber, blue is the data upon retraction. All data curves were horizontally shifted to make the zero in d (indicated by the black vertical line) correspond to the point where the cantilever deflection returns to zero after contact between the tip and fiber has been established.

interaction force gradient for the nominal ~2 N/m cantilever used.

After this jump to contact occurs, the z-piezo translator continues to advance until a user specified set-point force is reached. The tip indents into the fiber and the force on the cantilever changes from negative to positive, passing through the $q = 0$ condition until a preset force (in this case +5 nN) is reached. The extent of the indentation region (the distance between $d = 0$ and the value required to reach the set-point force) provides a quick and useful guide about the relative elastic modulus for the particular fiber under study. From Figure 2, it is clear that the indentation region for the polymer fibers extend to d values of +20 to +30 nm. When this occurs, the data indicate the tip is pressing into a soft surface (Young's modulus $\ll$1 GPa).

Once the set-point force is reached, the AFM controller withdraws the tip. The corresponding data are now colored blue. If the indentation is elastic, the blue retract data should overlap with the red indent data. The linearity of the unloading curves suggests that the tip radius was not significantly altered during the indentation. The absence of an overlap between approach and retract indicates the tip is subject to viscoelastic time-dependent forces that are a function of the prior indentation history as well as the rate of indentation, an unambiguous sign of an energy dissipative process.

As the tip continues to withdraw, the force exerted by the cantilever changes from positive to negative values, indicating that the tip adheres to the fiber surface. Normally, adhesive behavior persists until the restoring force of the downward bent cantilever snaps the tip off the fiber surface. For a clean tip/fiber interface, this jump off event is typically signified by a sharp discontinuity as the tip jumps back to the zero-force position. If the interface is well-defined, this typically occurs in the vicinity of $d = 0$. However, if an uncontrolled surface layer is present on the fiber, the tip does not jump off, but rather a gradual slides-off behavior is observed. The presence of an extended slide-off region might typically indicate a material "bridge" has formed between the tip and fiber surface. This is clearly the case observed for the synthetic fibers in Figure 2.

The longer the tip stays in contact with the fiber, the effect of an uncontrolled surface layer that overlays the base material tends to become more pronounced. The surface layer referred to in this context should be broadly considered. Such a layer could well be related to adsorbed water on the surface of the tip and/or fiber, or to unknown chemicals on the fiber surface, or to structural features (e.g., fibrillation at the nanoscale) that might decorate the surface of the fiber. Measurements at low RH are useful to assess the extent that adsorbed water plays in this slide-off behavior. Eventually, the bridge between tip and fiber breaks and the tip snaps off the fiber as the cantilever returns to its $F = 0$ position, indicating forces no longer are acting between the tip and fiber.

While no two $F(d)$ curves from the same fiber were exactly the same, it became clear during the course of this study that the $F(d)$ from each fiber had a characteristic shape with recognizable features. The composite graph plotted in Figure 2 allows a quick comparison between the interaction of an oxide ENP with different fibers and reveals a few systematic trends including:

(1) None of the fibers show an idealized $F(d)$ behavior (no hysteresis between approach and retract and a sharp snap off upon retraction) that would indicate a clean interface between the AFM tip and fiber surface. (2) All the data except that from Tyvek show a loading curve (red, approach) which does not overlap with the unloading data (blue, retract). This hysteretic behavior provides evidence that the fibers exhibit viscoelastic behavior even for small indentations. Presumably, this behavior is related to a relaxation of the near subsurface internal fiber structure as the load is increased. (3) The behavior of the $F(d)$ data for the synthetic fibers (polypropylene and polyester) are considerably different than observed for the natural cotton fibers in two important ways. First, the surface of the synthetic fibers appears significantly softer than the natural cotton fibers, and second, the synthetic fibers require a much larger retract distance (about 20 nm) for the AFM tip to release. Both these features suggest the synthetic fibers likely have a surface layer. (4) There is a significant difference in the $F(d)$ data between the two cotton fibers. The cotton fiber from the 100% cotton lab coat is softer than the cotton from the 80:20 poly cotton fabric. In addition, the cotton fiber from the 100% cotton lab coat exhibits a noticeable viscoelastic effect while the cotton from the 80:20 poly cotton fabric shows very little. Both cotton fibers show similar slide-off behavior, requiring displacements of the tip by 5 to 10 nm to finally effect a pull-off.

https://doi.org/10.1021/acs.langmuir.3c03939
Langmuir 2024, 40, 14788−14797

These observations suggest that the fabrics made from the cotton fibers have been manufactured and processed in different ways. We had no control or knowledge of any processing or surface treatments the fabrics may have received during the textile manufacturing and/or subsequent fabric/clothing fabrication steps. *A priori*, it is possible that residual surfactants, stabilizers, solvents, spinning agents, or plasticizers might unevenly coat individual fibers in the fabrics. This processing uncertainty places a constraint on the scope of the AFM work that can be performed.

Significant features in each curve also deserve further comment as summarized:

(1) The cotton fibers show a larger adhesive force upon retraction than the synthetic fibers, suggesting that oxide ENPs will more strongly adhere to cotton.

(2) $F(d)$ data taken on the fiber from the polypropylene fabric shows an extended indentation region. The z-piezo requires a displacement of nearly +35 nm before the 5 nN set-point is reached. This behavior, coupled with the extended slide-off behavior upon retraction indicates that the polypropylene fiber has a surface layer of unknown origin. See the SI for further evidence.

(3) $F(d)$ taken from the cotton fiber extracted from the 80:20 poly cotton fabric shows the largest jump to contact, suggesting the strongest attractive vdW force of all fibers studied.

(4) $F(d)$ taken from the polyester fiber extracted from the polycotton (80:20) fabric shows a similar behavior to that for polypropylene. Both synthetic fibers seem to exhibit effects attributed to an uncontrolled surface layer when compared to cotton.

(5) $F(d)$ taken from the Tyvek lab coat is closest to ideal and shows little hysteresis. The indentation region to reach the set-point force is small, extending only a few nanometers after contact is made. This indicates that Tyvek is the stiffest fabric studied.

(6) For a further discussion of data reproducibility, the challenges that the polyester fiber presented, and an estimate for the thickness of the uncontrolled surface layer on polypropylene, the reader is referred to the SI Figures S4–S6.

Adhesion Variation among Fabric. It is important to realize that the presence of nanoscale roughness in the surface topography of a fiber's surface can affect the contact between the tip and fiber during indentation, causing uncontrollable variations in the final results especially if the tip diameter is comparable to the surface roughness. For example, if the tip contacts a local topographic peak on the surface of the fiber, the nanoindentation depth could be larger as compared to the indentation of a flat surface with the same load. The reverse is also true. If the tip contacts a valley, the indentation depth could be lower than on a flat surface. Our images of fabric fibers included in SI Figure S2 taken under high magnification show mostly smooth or flat surface. A low level of variation in the final adhesion results can be expected

Furthermore, the measured adhesion does not take into account any additional trapping that may occur when an ENP becomes wedged between the woven yarn of a fabric. This trapping process could well produce an adhesive force many times stronger than what we measure. Rather, we are interested in the intrinsic forces that hold the tip to the fiber surface, rather than any geometrical effects that may occur when an ENP becomes wedged into a fabric.

The maximum adhesion force from each curve in Figure 2 is well-defined and the results are tabulated in Table 2. To provide a statistical estimate of the maximum adhesion force of the SiO_x tip to each fiber, multiple $F(d)$ data were taken on each of the fibers at three nominal set-point values of 2, 5, and 10 nN. The measured adhesive forces from these separate experiments were equally weighted to find an average value for the lift-off force. These averaged results are also tabulated in Table 2 and provide an indication of the spread in the measured adhesion values. For the data plotted in Figure 2, Tyvek shows the smallest adhesion, while the two cotton fibers, one from the 100% cotton fabric and the other from the 80:20 poly cotton fabric, have the highest adhesion.

Table 2. A List of Adhesive Forces of the SiO_x Tip to Each Fiber as Obtained from $F(d)$ Data[a]

fabric	F_{ad} (nN)[b]	average F_{ad} (nN)
Tyvek (HDPE)	1.9	2.7 ± 1.0 (n = 6)
polypropylene	2.7	2.4 ± 0.4 (n = 6)
polyester (PET) (from 80:20 polycotton)	2.9	3.3 ± 0.4 (n = 9)
100% cotton	3.7	3.1 ± 0.3 (n = 9)
cotton (from 80:20 polycotton)	6.0	5.9 ± 1.2 (n = 9)

[a]Two data sets are listed. The values for F_{ad} are from the data in Figure 2. The average value for F_{ad} (listed along with the standard deviation) is the average obtained from a sequence of $F(d)$ measurements. [b]Data from Figure 2.

From the data in Table 2, the relative ordering of the maximum adhesion between the oxidized SiO_x AFM tip (14 nm diam.) and the individual fabric fibers seems to roughly correlate with the gravimetric assessment of adhesion measurements deduced from the mass change upon fabric shaking previously reported.[4]

Effect of Humidity on Adhesion. After completing the $F(d)$ measurements under ambient conditions, the metal box enclosure surrounding the AFM was purged with dry N_2 gas. This procedure allowed an investigation of whether a thin layer of water strongly influenced the adhesion of the AFM tip to each fabric fiber. Once a RH < 2% was reached, a parallel set of $F(d)$ measurements were made, mirroring those already performed under ambient conditions. Of the five fibers studied, only the two cotton fibers required a significant realignment of the AFM cantilever over the fiber because of a noticeable change in the position of the cotton fiber due to a change in RH, a result presumably related to the dehydration of the cotton fibers. $F(d)$ data at ambient and reduced humidity for each fiber is plotted in Figure 3. The data at low RH is offset by a fixed amount for clarity. The ambient RH listed on each plot is the lab room humidity measured on the day of the experiment.

Data for the Tyvek fiber are plotted in Figure 3(a). The data indicate the release of the tip from the Tyvek surface is not significantly affected by a change in RH.

The two cotton fibers are compared in Figure 3(b),(c). Examination of this data shows that a reduction in RH modifies some features in the withdrawal data plotted in blue. In particular, the gradual tip "slide-off" region observed upon retraction from both cotton fibers seems to be reduced as the RH is decreased. The adhesive forces however are not

https://doi.org/10.1021/acs.langmuir.3c03939
Langmuir 2024, 40, 14788−14797

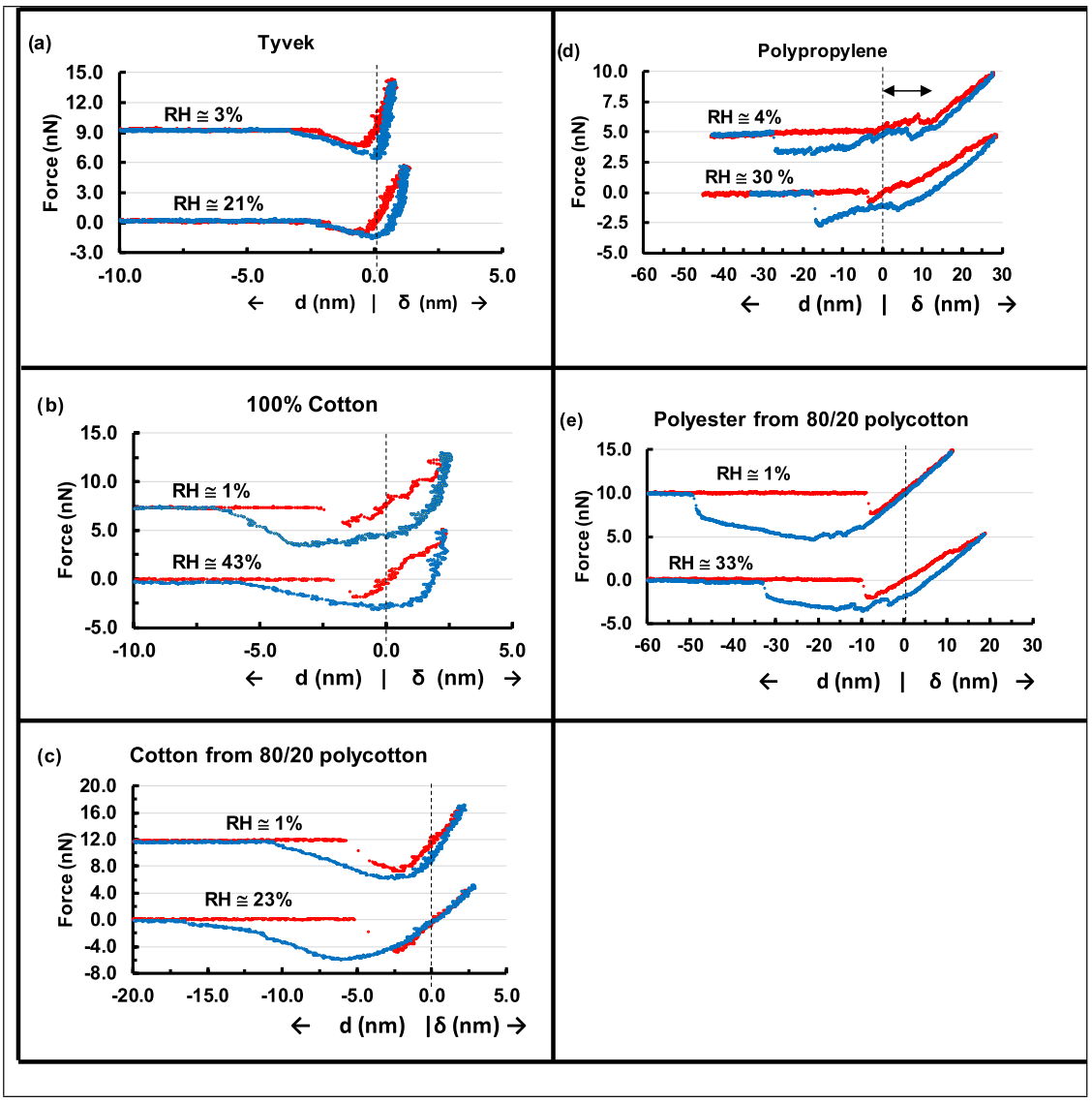

Figure 3. A comparison of $F(d)$ data at ambient and low RH conditions for a SiO_x AFM tip on (a) the Tyvek surface; (b) a cotton fiber extracted from the 100% cotton fabric; (c) a cotton fiber extracted from the 80:20 poly cotton fabric; (d) a fiber from the polypropylene fabric; and (e) a polyester fiber extracted from the 80:20 poly cotton fabric. The nominal loading force in all experiments was 5 nN. The low RH data are shifted upward by a constant offset to facilitate a comparison. For both the synthetic polypropylene and polyester fibers, the "slide-off" region in the $F(z)$ data becomes noticeably extended by ∼15 nm as the RH is decreased.

significantly affected in either cotton fiber by the reduction in RH.

As for the case of cotton fibers, the measured adhesive force for polypropylene and polyester fibers (see Figure 3(d),(e)) are not significantly decreased by a reduction in RH. Of all the fibers studied, the polyester fiber showed the largest change in adhesion as the humidity was reduced. Figure 3(e) shows that the polyester fiber showed an increase in the adhesive force, increasing from 3.6 nN under ambient conditions to 5.4 nN when the RH is near 0%. This results in a 2.8 nN increase in the maximum adhesive force as the RH is decreased.

The spontaneous formation of a water capillary bridge for a finite RH is expected to more tightly bind an ENP under ambient conditions. As described in the literature,[31,32] the magnitude of the capillary force binding a spherical nanoparticle to a flat surface depends on the nanoparticle radius, the RH, and the two contact wetting angles of the microscopic water bridge between an ENP and the substrate. The AFM tip (with nanoscale radius of curvature) is treated as an effective oxide nanoparticle that is hydrophilic and should have a low water contact angle (WCA). The WCA to each of the fabric fibers is more difficult to estimate. Since cotton absorbs water, no capillary bridge should form between the AFM tip and cotton fiber. Thus, *a priori*, one might expect the liftoff force of an oxide ENP from a cotton fiber should be independent of RH. This expectation is consistent with the data in Figure 3(b),(c).

Regarding the synthetic fibers, their low absorbency of water suggests that these fibers can support an adsorbed water layer in equilibrium with the ambient RH. The C−C and C−H bonds in the precursor hydrocarbon molecules are not significantly polar, so polymers derived from these nonpolar molecules also tend to be nonpolar (hydrophobic) themselves. Of the three synthetic fibers studied, polyester (poly(ethylene terephthalate), PET) is the most polar and thus should exhibit the highest hydrophilic tendencies, while Tyvek and

https://doi.org/10.1021/acs.langmuir.3c03939
Langmuir 2024, 40, 14788−14797

polypropylene are the least polar and should be more hydrophobic. To make these synthetic fibers strongly hydrophilic would require additional surface treatments.

In prior work[4] water contact angles were measured using the same synthetic fabrics studied here. In contrast to cotton which readily absorbs water, the synthetic Tyvek and polypropylene fabrics were found to be hydrophobic with static WCAs near 120°. Water contact angle (WCA) measurements for the 80:20 polycotton fabric were also attempted, but the cotton in the fabric absorbed the water drop. For this reason, the water contact angle for the 80:20 polycotton could not be measured.

Idealized analytical models found in the literature[30,31] provide useful guidelines to predict the expected increase in adhesive force due to formation of a capillary bridge. Thus, when a hydrophilic ENP is supported by a hydrophilic substrate, a significant increase in the lift-off force (typically 20−30 nN) is expected when the RH is ∼20% or higher. This consideration is perhaps most applicable to the polyester fiber, providing a rough estimate for the expected change in lift-off force of the AFM tip from a polyester fabric fiber as the RH is reduced to near zero.

The data in Figure 3 show only small changes in the measured maximum adhesion as the RH is reduced from ambient conditions to near 0% for all three synthetic fibers. Admittedly, the upper limit of RH we investigated was limited to ambient laboratory room values, typically less than 30%. The largest change in adhesive force as the RH varied was observed for the polyester fiber (Figure 3(e)), but the observed change is opposite to what is expected if a water capillary bridge forms. Thus, if a water layer is present, it evidently does not play a major role in adhesion of the AFM tip to the different synthetic fibers for the conditions studied.

CONCLUSIONS

This study obtained information about the interaction of an oxide AFM tip with different cotton, polypropylene, polyester, and Tyvek (HD polyethylene) fibers extracted from fabrics commonly used in the manufacture of protective laboratory clothing. The goal was to search for clues that might be useful to further optimize the adhesion of nanometer-size ENPs to different fabrics. This study provided (i) systematic information that allows a comparison of the interaction of an AFM tip with different fabric fiber surfaces, (ii) no evidence for a significant triboelectric charging effect after an AFM tip contacts a fabric fiber, (iii) no evidence for increased adhesion due to the formation of a water capillary bridge when an AFM tip contacts different fabric fibers under typical laboratory RH conditions, (iv) clear evidence for viscoelastic behavior when an AFM tip contacts different fabric fibers, (v) evidence that two cotton fibers extracted from two different fabrics interact differently with an AFM tip, implying that fabric manufacturing processes can play an important role in adhesion, and (vi) evidence for an extended slide off behavior in the removal of an AFM tip, especially from the synthetic polypropylene and polyester fabric fibers. This behavior can be attributed to an uncontrollable surface layer that coats the base polymer fibers used to manufacture these fabrics.

In the absence of significant electrostatic and capillary bridge forces, it seems safe to conclude that the main force governing the noncontact interaction between an oxide ENP and the different fabrics under study is the van der Waals force. The strength of the vdW force describes the attractive interaction between an oxide ENP of diameter 2R (mimicked by the AFM tip) and each fabric fiber as a function of the surface-to-surface separation d. The functional form of the vdW interaction when the surface of a sphere of radius R is held a distance d above a flat substrate is given by eq 2.

$$F_{\mathrm{vdW}} = -\frac{H_{12}R}{6d^2} \tag{2}$$

where H_{12} is the Hamaker constant. Equation 2 is valid when $R \gg d$. The relative magnitudes of the jump to contact discontinuity in Figure 2 indicate that H_{12} for Tyvek, polypropylene and polyester fibers are comparable while H_{12} for the cotton fibers are larger, indicating that an oxide ENP will be more likely attracted to cotton fibers than to synthetic ones.

This result is consistent with prior work[4] which found that alumina ENPs bind weakly to Tyvek and strongest to cotton, with the synthetic fabrics polypropylene and polyester falling in between. This conclusion was reached by controllably exposing fabric swatches to alumina nanoparticles having a broad size distribution (diameters between 10 nm and 1 μm). Following exposure, standard gravimetric techniques were used to measure the mass change of fabric swatches before and after shaking. Tyvek showed the largest mass change, indicating a weak binding of alumina ENPs. Cotton had the smallest mass change upon shaking which indicates a relatively stronger binding. Although we did not investigate Al_2O_3 ENPs in this AFM study, we found roughly the same trend by measuring the adhesion of a 14 nm diameter SiO_x AFM tip to fabric fibers extracted from the same lab coat fibers.

From everyday experience, it is known that electrostatic cling can cause the attraction and adhesion of a variety of different materials to fabrics. Therefore, one issue we addressed was what role, if any, electrostatic forces play in attracting ENPs to a fabric. The situation likely to produce the largest effect is when the SiO_x tip is touched to polypropylene or polyethylene (Tyvek), since these materials typically lie on opposite ends of the triboelectric series.[33] No evidence was found under either ambient or reduced humidity conditions to suggest that any long-range forces developed after multiple tip touches to polypropylene or Tyvek fabrics under study. This implies that triboelectric charge transfer between an ENP and a fabric, or the presence of patch charges on the fabric itself, are likely negligible compared to other forces that act.

Analysis of the $F(d)$ data for all fibers indicates the adhesion force of the tip to the fiber is only affected in a subtle way as the humidity is reduced from ambient to near zero. If a capillary water bridge forms under ambient conditions, a significant increase in the lift-off force of ∼20 nN or more should have occurred as the RH changed from near zero to ambient. No such increase was observed. Additional AFM studies using higher RH would be useful to confirm this trend.

It was found that the $F(d)$ data from the two cotton fibers, one extracted from the 100% cotton fabric, the other from the 80:20 polycotton fabric, were quite different. The cotton fiber from the 80:20 polycotton exhibits a strong vdW force of attraction to the AFM tip, while the attractive force of the cotton fiber from the 100% cotton lab coat is weaker. This implies that by controlling some currently unknown fabric processing step, ENP adhesion can be modified.

Finally, the significant viscoelastic behavior observed for all the fabric fibers except Tyvek suggest alternate routes to producing a stronger adhesion of ENPs to fabrics. The viscoelastic behavior influencing lift-off appears to fall into two

https://doi.org/10.1021/acs.langmuir.3c03939
Langmuir 2024, 40, 14788−14797

broad categories: an extended lift-off separation for the synthetic polypropylene and polyester and a shorter lift-off behavior for the natural fibers made from cotton. The extended lift-off regime is suggestive of chain pulling effects that are expected for polymer materials. From our work, there is also some evidence that the maximum adhesive force increases with the AFM cantilever set point force. Thus, it is possible that following ENP exposure, the adhesion of ENPs to clothing might be increased by physically compressing the fabric (such as folding when stored) instead of simply hanging.

Taken together as a whole, this study of AFM tip-fabric interactions illustrates the information that can be gleaned about the interaction of ENPs with protective clothing fabric. The impact of our work is that it promotes the view that fabrics constitute a unique materials class with different properties that can be further tailored by structure modifications such as additional surface chemical treatments which may alter functionality and hydrophobicity of the fabric fibers. In this way, our work provides some much needed groundwork that may promote further studies to better design smart textiles to meet future needs.

■ ASSOCIATED CONTENT

Supporting Information

The Supporting Information is available free of charge at https://pubs.acs.org/doi/10.1021/acs.langmuir.3c03939.

(a) SEM images of the fabrics, (b) SEM images of a fiber surface, (c) Tip alignment issues, (d) The reproducibility of $F(z)$ data, (e) The special case of polyester fibers, and (f) Penetrating the uncontrolled surface layer on polypropylene (PDF)

■ AUTHOR INFORMATION

Corresponding Author

Candace Su-Jung Tsai − *Department of Environmental Health Sciences, Fielding School of Public Health, University of California, Los Angeles, California 90095, United States;* orcid.org/0000-0002-7296-8278; Email: candacetsai@ucla.edu

Author

Ronald G. Reifenberger − *Department of Physics, Purdue University, West Lafayette, Indiana 47907, United States*

Complete contact information is available at: https://pubs.acs.org/10.1021/acs.langmuir.3c03939

Author Contributions

The manuscript was written through contributions from all authors.

Funding

This research was funded by the Department of Health and Human Services, Center for Disease Control and Prevention, Grant No. 1 R21OH011507−01.

Notes

The authors declare no competing financial interest.

■ ACKNOWLEDGMENTS

The authors wish to thank Aigerim Maksot for her help with the initial preparation of the lab coat materials, and Yi-Hsuan (Amelia) Chen for her help taking additional SEM images of the lab coat materials. RR would like to thank Prof. Ryan Wagner for insightful discussions about AFM throughout this study.

■ ABBREVIATIONS

AFM, atomic force microscope; DMT, Derjaguin−Müller−Toporov; ENP, engineered nanoparticles; HD, high density; HVAC, heating, ventilation, and air conditioning; invOLS, inverse optical lever sensitivity; NIOSH, National Institute for Occupational Safety and Health; RH, relative humidity; SI, supporting information; vdW, van der Waals; WCA, water contact angle

■ REFERENCES

(1) Thangavel, P.; Park, D.; Lee, Y.-C. Recent Insights into Particulate Matter (PM2.5)-Mediated Toxicity in Humans: An Overview. *Int. J. Environ. Res. Public Health* **2022**, *19* (12), No. 7511.

(2) Rezaei, M.; Johnson, M. S. Airborne Nanoparticles: Control and Detection. In *Encyclopedia of Sustainability Science and Technology*; Meyers, R. A., Ed.; Springer: New York, 2020; pp 1−49.

(3) Dolez, P. I.; Marsha, S.; McQueen, R. H. Fibers and Textiles for Personal Protective Equipment: Review of Recent Progress and Perspectives on Future Developments. *Textiles* **2022**, *2* (2), 349−381.

(4) Maksot, A.; Sorna, S. M.; Blevens, M.; Reifenberger, R. G.; Hiyoto, K.; Fisher, E. R.; Vindell, T.; Li, Y. V.; Kipper, M. J.; Tsai, C. S.-J. Engineered Nanoparticle Release from Personal Protective Clothing: Implications for Inhalation Exposure. *ACS Appl. Nano Mater.* **2022**, *5* (2), 2558−2568.

(5) Hiyoto, K.; Sorna, S. M.; Maksot, A.; Reifenberger, R. G.; Tsai, C. S.-J.; Fisher, E. R. Effects of Surface Hydrophobicity of Lab Coat Fabrics on Nanoparticle Attachment and Resuspension: Implications for Fabrics Used for Making Protective Clothing or Work Uniform. *ACS Appl. Nano Mater.* **2023**, *6* (9), 7384−7394.

(6) Wei, Q. F.; Wang, X. Q. AFM Characterisation of Technical Fibres. *J. Ind. Text.* **2004**, *34* (1), 51−60.

(7) Drummond, C. J.; Senden, T. J. Examination of the geometry of long-range tip—sample interaction in atomic force microscopy. *Colloids Surf., A* **1994**, *87* (3), 217−234.

(8) Todd, B. A.; Eppell, S. J. Probing the Limits of the Derjaguin Approximation with Scanning Force Microscopy. *Langmuir* **2004**, *20* (12), 4892−4897.

(9) Sokolov, I.; Ong, Q. K.; Shodiev, H.; Chechik, N.; James, D.; Oliver, M. AFM study of forces between silica, silicon nitride and polyurethane pads. *J. Colloid Interface Sci.* **2006**, *300* (2), 475−481.

(10) Binnig, G.; Quate, C. F.; Gerber, C. Atomic Force Microscope. *Phys. Rev. Lett.* **1986**, *56* (9), 930−933.

(11) Magonov, S. N.; Reneker, D. H. Characterization of polymer surfaces with atomic force microscopy. *Annu. Rev. Mater. Sci.* **1997**, *27* (1), 175−222.

(12) Wang, D.; Russell, T. P. Advances in Atomic Force Microscopy for Probing Polymer Structure and Properties. *Macromolecules* **2018**, *51* (1), 3−24.

(13) Canetta, E.; Montiel, K.; Adya, A. K. Morphological changes in textile fibres exposed to environmental stresses: Atomic force microscopic examination. *Forensic Sci. Int.* **2009**, *191* (1), 6−14.

(14) Zimmerman, B.; Chow, J.; Abbott, A. G.; Ellison, M. S.; Kennedy, M. S.; Dean, D. Variation of Surface Charge along the Surface of Wool Fibers Assessed by High-Resolution Force Spectroscopy. *J. Eng. Fibers Fabr.* **2011**, *6* (2), No. 37827887.

(15) Naebe, M.; Haque, A. N. M. A.; Haji, A. Plasma-Assisted Antimicrobial Finishing of Textiles: A Review. *Engineering* **2022**, *12*, 145−163.

(16) Gashti, M. P.; Alimohammadi, F.; Song, G.; Kiumarsi, A. Characterization of nanocomposite coatings on textiles: A brief review on Microscopic technology. *Curr. Microsc. Contrib. Adv. Sci. Technol.* **2012**, *2*, 1424−1437.

(17) Behary, N.; Perwuelz, A. Atomic Force Microscopy − For Investigating Surface Treatment of Textile Fibers. In *Atomic Force*

Microscopy - Imaging, Measuring and Manipulating Surfaces at the Atomic Scale; Victor, B., Ed.; IntechOpen, 2012.
(18) Koc, S. K. Applications of Atomic Force Microscopy in Textiles. *J. Eng. Fibers Fabr.* **2015**, *10* (1), No. 139849442.
(19) Luo, X.; Weng, Y.; Wang, S.; Du, J.; Wang, H.; Xu, C. Superhydrophobic and oleophobic textiles with hierarchical micro-nano structure constructed by sol−gel method. *J. Sol−Gel Sci. Technol.* **2019**, *89* (3), 820−829.
(20) Nakamura, T.; Mondarte, E. A. Q.; Tahara, H.; Chang, R.; Hayashi, T. Chemical force spectroscopic mapping of nanoparticle-embedded polyester fiber by atomic force microscopy. *Mol. Cryst. Liq. Cryst.* **2021**, *728* (1), 52−58.
(21) Baranova, O. N.; Zolina, L. I. Atomic-Force Microscopy Study of Cotton Cloth Modified by Silver Nanoparticles. *Fibre Chem.* **2022**, *54* (1), 51−53.
(22) Salem, R. T. A.; Thompson, K.; Uttamlal, M. Bleaching cotton in textile conservation: a closer look using atomic force microscopy. *Heritage Sci.* **2022**, *10* (1), 195.
(23) Maragliano, C.; Glia, A.; Stefancich, M.; Chiesa, M. Effective AFM cantilever tip size: methods for in-situ determination. *Meas. Sci. Technol.* **2015**, *26* (1), No. 015002.
(24) Higgins, M. J.; Proksch, R.; Sader, J. E.; Polcik, M.; Endoo, S. M.; Cleveland, J. P.; Jarvis, S. P. Noninvasive determination of optical lever sensitivity in atomic force microscopy. *Rev. Sci. Instrum.* **2006**, *77* (1), No. 0133701.
(25) Sader, J. E.; Sanelli, J. A.; Adamson, B. D.; Monty, J. P.; Wei, X.; Crawford, S. A.; Friend, J. R.; Marusic, I.; Mulvaney, P.; Bieske, E. J. Spring constant calibration of atomic force microscope cantilevers of arbitrary shape. *Rev. Sci. Instrum.* **2012**, *83* (10), No. 103705.
(26) Butt, H.-J.; Cappella, B.; Kappl, M. Force measurements with the atomic force microscope: Technique, interpretation and applications. *Surf. Sci. Rep.* **2005**, *59* (1), 1−152.
(27) Chizhik, S. A.; Huang, Z.; Gorbunov, V. V.; Myshkin, N. K.; Tsukruk, V. V. Micromechanical Properties of Elastic Polymeric Materials As Probed by Scanning Force Microscopy. *Langmuir* **1998**, *14* (10), 2606−2609.
(28) Cappella, B. *Mechanical Properties of Polymers Measured through AFM Force-Distance Curves*; Springer: Cham, 2016.
(29) Cappella, B.; Dietler, G. Force-distance curves by atomic force microscopy. *Surf. Sci. Rep.* **1999**, *34* (1), 1−104.
(30) Reifenberger, R. *Fundamentals of Atomic Force Microscopy*; World Scientific, 2015.
(31) Butt, H.-J.; Kappl, M. Normal capillary forces. *Adv. Colloid Interface Sci.* **2009**, *146* (1), 48−60.
(32) Sedin, D. L.; Rowlen, K. L. Adhesion Forces Measured by Atomic Force Microscopy in Humid Air. *Anal. Chem.* **2000**, *72* (10), 2183−2189.
(33) Zou, H.; Guo, L.; Xue, H.; Zhang, Y.; Shen, X.; Liu, X.; Wang, P.; He, X.; Dai, G.; Jiang, P.; et al. Quantifying and understanding the triboelectric series of inorganic non-metallic materials. *Nat. Commun.* **2020**, *11* (1), No. 2093.

https://doi.org/10.1021/acs.langmuir.3c03939
Langmuir 2024, 40, 14788−14797